2016

Oxygen Mass Transport in Stented Coronary Arteries

Eoin Murphy

Adrian S. Dunne

David Martin

See next page for additional authors

Authors

Eoin Murphy, Adrian S. Dunne, David Martin, and Fergal Boyle

BMES
BIOMEDICAL ENGINEERING SOCIETY™
www.bmes.org

CrossMark

Medical Stents: State of the Art and Future Directions

Oxygen Mass Transport in Stented Coronary Arteries

EOIN A. MURPHY [ORCID],[1] ADRIAN S. DUNNE,[2] DAVID M. MARTIN,[1] and FERGAL J. BOYLE[1]

[1]School of Mechanical and Design Engineering, Dublin Institute of Technology, Bolton St, Dublin 1, Ireland; and [2]CADFEM Ireland Ltd, 18 Windsor Place, Lower Pembroke St, Dublin 2, Ireland

Associate Editor Peter McHugh oversaw the review of this article.

Abstract—Oxygen deficiency, known as hypoxia, in arterial walls has been linked to increased intimal hyperplasia, which is the main adverse biological process causing in-stent restenosis. Stent implantation has significant effects on the oxygen transport into the arterial wall. Elucidating these effects is critical to optimizing future stent designs. In this study the most advanced oxygen transport model developed to date was assessed in two test cases and used to compare three coronary stent designs. Additionally, the predicted results from four simplified blood oxygen transport models are compared in the two test cases. The advanced model showed good agreement with experimental measurements within the mass-transfer boundary layer and at the luminal surface; however, more work is needed in predicting the oxygen transport within the arterial wall. Simplifying the oxygen transport model within the blood flow produces significant errors in predicting the oxygen transport in arteries. This study can be used as a guide for all future numerical studies in this area and the advanced model could provide a powerful tool in aiding design of stents and other cardiovascular devices.

Keywords—Coronary artery disease, Stents, In-stent restenosis, Hypoxia, Computational fluid dynamics.

INTRODUCTION

Coronary artery disease is characterized by the development of atherosclerotic lesions within the walls of coronary arteries. Percutaneous coronary intervention is used throughout the world as a fast and effective treatment for coronary artery disease. Typically, the procedure involves the expansion of a stent at a lesion site by a balloon-tipped catheter, thereby dilating a previously narrowed artery. In some cases re-narrowing of the ar-

tery, known as in-stent restenosis (ISR), occurs and is primarily caused by the development of intimal hyperplasia (IH). Drug eluting stents (DESs) have reduced the frequency of ISR to single digit percentages; however, by affecting the natural biological healing processes within the arterial wall, DESs mask the underlying adverse consequences of the stenting procedure which can lead to late-stent thrombosis.[1] The biological processes that can result in ISR are instigated by the effects of stent implantation and include structural damage to the arterial wall, augmentation of the local haemodynamic environment and the presence of a foreign body.[20] In terms of the augmentation of the haemodynamic environment, stenting produces a predominantly beneficial effect, i.e., restoration of required blood flow to downstream vasculature; however, locally within the stented region, the haemodynamics impact the natural healing processes within the arterial wall. This local augmentation of the haemodynamic environment due to the presence of a stent in turn affects the oxygen flux into the arterial wall which can result in a deficiency of oxygen, known as hypoxia, in some regions. Hypoxia has been associated with increased adventitial vasa vasorum[6] and IH in animal studies.[24,26] Therefore, given that hypoxia and increased IH may result in ISR, investigation of the local oxygen transport within stented artery models using computational fluid dynamics (CFD) is important in order to elucidate the effects of stenting on the arterial wall cellular components and also to aid in the design of future coronary stents.

Hypoxia is known to cause atherosclerosis in large arteries.[29] Because of this, the majority of numerical studies of oxygen transport in three-dimensional (3D) arteries have been in relation to arteries with no implanted device. Many of these numerical studies fall into the category of wall-free models where only the

---

Address correspondence to Eoin A. Murphy, School of Mechanical and Design Engineering, Dublin Institute of Technology, Bolton St, Dublin 1, Ireland. Electronic mail: eoin.murphy@dit.ie

oxygen transport in the blood is modeled and a constant value of oxygen concentration is specified on the luminal surface.[7] Another category of oxygen transport studies employs fully coupled blood and arterial wall models, where diffusion and consumption of oxygen in the arterial wall are modeled, and a constant flux or concentration boundary condition is specified on the media/adventitia boundary interface.[2,28] These models offer the advantage of a more realistic representation of the oxygen transport conditions; however, in these simulations the arterial wall was modeled as homogeneous which is not physiologically correct. In contrast, Richardson modeled the oxygen transport within heterogeneous coronary arterial walls only, with varying parameters according to age and stenosis, while ignoring the flow within the lumen.[23] To date, the computational modeling of oxygen transport in stented coronary arteries has only been undertaken by Caputo et al.[2] Their study allowed direct comparison of in silico models, predicting the haemodynamic and oxygen transport conditions, with observations of neointimal hyperplasia obtained from the porcine coronary artery. This study concluded that stent implantation does significantly alter the local haemodynamic conditions and the oxygen transfer; however, because of limitations in the oxygen transport model adopted, it is possible that the extent of the hypoxic regions in the arterial wall was under-predicted.

Oxygen is carried in the blood in two forms: free oxygen dissolved in the plasma and oxygen reversibly-bound to hemoglobin, known as oxyhemoglobin, contained within red blood cells (RBCs). RBCs are subjected to a shear-dependent dispersion within blood flow that accordingly affects the oxygen transport within the blood.[5,8] The above studies ignore the transportation of the bound oxygen in their models. The limitation of ignoring the bound oxygen was analyzed in Moore and Ethier's 2D study of oxygen transport in large arteries.[19] They made the important conclusion that ignoring the bound oxygen produces large errors in oxygen transport predictions.

In this work oxygen transport within stented coronary arteries was investigated using the most advanced blood oxygen transport model presented to date and, significantly, includes the bound oxygen. The model was first evaluated using two test cases and subsequently used to assess the arterial wall oxygenation in three realistically-deformed stented arteries. Additionally, in two test cases, four simplified oxygen transport models are compared with the most advanced model in order to assess their limitations. The results of this study give strong evidence that simplifying the blood oxygen transport model has significant effects on predicting the resulting oxygen tension within the arterial wall and, critically, should provide a comprehensive framework for all future oxygen modeling studies in human arteries.

METHODOLOGY

Background

Blood consists of liquid plasma in which three types of cellular elements are suspended: RBCs, white blood cells and platelets. RBCs constitute about 45%, by volume, of whole blood and are the main carriers of oxygen. The coronary arteries act as a conduit for the blood to deliver oxygen and nutrients to the heart muscle downstream. Oxygen is critical for the maintenance of arterial wall physiology and is supplied to the cells within the arterial wall from both the luminal blood and blood passing through vasa vasorum in the adventitia. Oxygen is transported in blood as free oxygen dissolved in plasma and oxygen reversibly-bound to hemoglobin within the RBCs.

Blood Oxygen Transport

The concentration of free oxygen dissolved in plasma is quantified by the oxygen tension, i.e. the partial pressure of oxygen in plasma. The oxygen tension is related to the free oxygen concentration by Henry's law:

$$PO_2 = \frac{C}{\alpha} \quad (1)$$

where PO_2 is the oxygen tension, α is the solubility of oxygen in plasma, and C represents the concentration of free oxygen in plasma. The amount of bound oxygen contained in the RBCs in the form of oxyhemoglobin is proportional to the PO_2 within the surrounding plasma and can be approximated using the Hill equation (oxygen dissociation curve, as shown in Fig. 1a):

$$S = \frac{PO_2^n}{PO_2^n + PO_{2,50}^n} \quad (2)$$

where S is the ratio of oxyhemoglobin to total hemoglobin in the RBCs (commonly expressed as a percentage), $PO_{2,50}$ is the PO_2 value at which the hemoglobin is 50% saturated and n is the Hill parameter. For the purpose of modeling oxygen transport in blood, difficulty arises when the bound oxygen is included in the model because of the non-linear nature of the Hill equation. When included, the transportation of both free oxygen and bound oxygen in the blood can be modeled using two advection–diffusion equations given as Eqs. (3) and (4) respectively:

$$\alpha \frac{\mathcal{D}PO_2}{\mathcal{D}t} = \alpha \nabla.(D_b \nabla PO_2) + r \quad (3)$$

$$[Hb] \frac{\mathcal{D}S}{\mathcal{D}t} = [Hb] \nabla.(D_c \nabla S) - r \quad (4)$$

where $\mathcal{D}/\mathcal{D}t$ is the substantial derivative, D_b is the diffusivity of free oxygen in the blood, r is the rate of release of oxygen from the hemoglobin, [Hb] is the total oxygen carrying capacity of hemoglobin in blood, and D_c is the diffusivity of oxyhemoglobin in blood. [Hb] is assumed to be constant, thus ignoring the plasma skimming layer which has little effect on the oxygen transport.[19] Oxyhemoglobin is encapsulated in RBCs and therefore the D_c value is interpreted as the shear-augmented dispersion coefficient of RBCs in blood flow. In previous studies this value is taken as 1.5×10^{-11} m^2/s,[19] which is the dispersion coefficient for red tracer cells in a straight glass tube at an approximate shear rate of 20 s^{-1}.[3] Higher shear rates are encountered in carotid and coronary arteries and therefore, a variable dispersion coefficient was employed in this work. This was extrapolated from three separate studies by Goldsmith, Goldsmith and Marlow, and Cha and Beissinger as described in Eqs. (5) and (6) with the resultant D_c plotted against the shear rate shown in Fig. 1b:[5,10,11]

$$\text{For } 0 \leq \dot{\gamma} \leq 100 s^{-1} : D_c = 5.00 \times 10^{-12} + 5.00 \times 10^{-13}\dot{\gamma} \tag{5}$$

$$\text{For } \dot{\gamma} > 100 s^{-1} : D_c = 3.68 \times 10^{-11} + 1.96 \times 10^{-13}\dot{\gamma} \tag{6}$$

where $\dot{\gamma} = \sqrt{2\mathbf{D} : \mathbf{D}}$ is the local shear rate and $\mathbf{D}$ is the strain rate tensor. The two constants used in Eq. (5) are deduced from RBC ghost cell experiments by Goldsmith, and Goldsmith and Marlow between average shear rates of 2–20 s^{-1} at haematocrits of 39 and 40% respectively.[10,11] The two constants used in Eq. (6) were deduced from the shear-induced particle diffusivity calculated by Cha and Beissinger at shear rates between 200 and 1000 s^{-1} at a RBC ghost volume fraction of 0.45 corresponding to the average haematocrit for a human male.[5]

To reduce complexity when performing numerical simulations the two advection–diffusion equations given above can be added together to form a single equation, as described in Moore and Ethier[19]:

$$\left(1 + \frac{[\text{Hb}]}{\alpha}\frac{dS}{dPO_2}\right)\frac{\mathcal{D}PO_2}{\mathcal{D}t} = \nabla \cdot \left[\left(D_b\left(1 + \frac{[\text{Hb}]}{\alpha}\frac{D_c}{D_b}\frac{dS}{dPO_2}\right)\right)\nabla PO_2\right] \tag{7}$$

where the term dS/dPO_2, as shown in Fig. 1c, is the slope of the oxygen dissociation curve given by:

$$\frac{dS}{dPO_2} = \frac{1}{PO_{2,50}^n}\frac{nPO_2^{n-1}}{\left[1 + \left(PO_2/PO_{2,50}\right)^n\right]^2}. \tag{8}$$
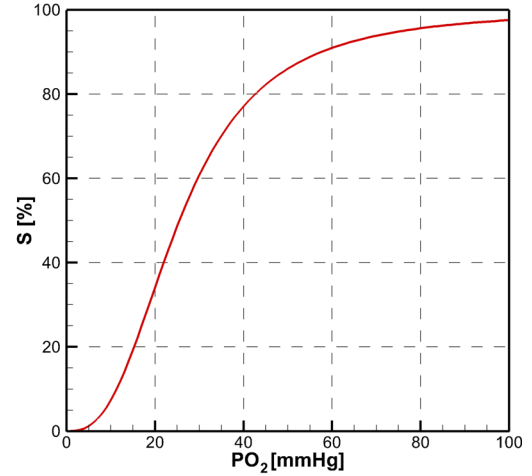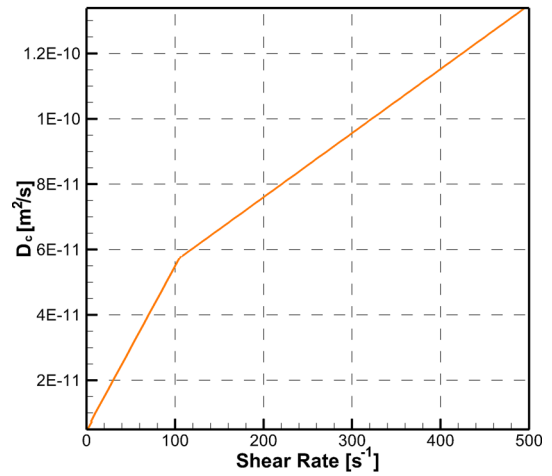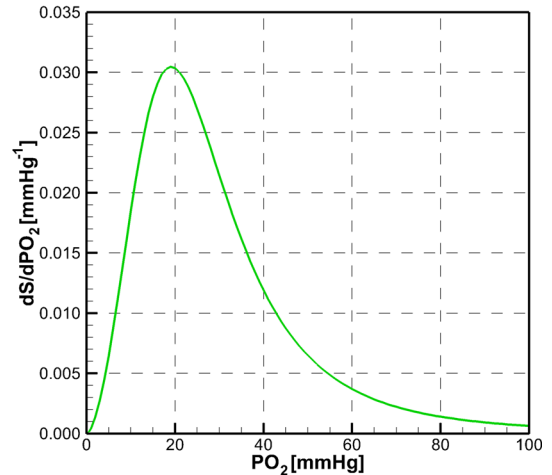
(a) **Oxygen Dissociation Curve**

(b) **D_c vs Shear Rate**

(c) **dS/dPO$_2$ vs PO$_2$**

FIGURE 1. (a) Oxygen dissociation curve for *n* = 2.7, (b) D_c as extrapolated from experimental studies for the shear rates ranging from 1 to 500 s^{-1}, and (c) the gradient, *d*S/*d*PO$_2$, of the oxygen dissociation curve plotted against PO$_2$.

Given the shape of the oxygen dissociation curve, non-linearity enters the oxygen transport equation through this term. In order to implement Eq. (7) in the commercially-available CFD software package used here it must be rearranged into the form given in Eq. (9):

$$\frac{\mathcal{D}\mathrm{PO}_2}{\mathcal{D}t} = \nabla.[D'\nabla\mathrm{PO}_2] + \{\text{Source}\} \qquad (9)$$

where the diffusivity coefficient D' and the source term {Source} are given in Eqs. (10) and (11) respectively:

$$D' = \left(D_b\left(1 + \frac{[\mathrm{Hb}]}{\alpha}\frac{D_c}{D_b}\frac{d\mathrm{S}}{d\mathrm{PO}_2}\right)\right) \bigg/ \left(1 + \frac{[\mathrm{Hb}]}{\alpha}\frac{d\mathrm{S}}{d\mathrm{PO}_2}\right) \qquad (10)$$

$$\text{Source} = \left[D_b\left(1 + \frac{[\mathrm{Hb}]}{\alpha}\frac{D_c}{D_b}\frac{d\mathrm{S}}{d\mathrm{PO}_2}\right)\bigg/\left(1 + \frac{[\mathrm{Hb}]}{\alpha}\frac{d\mathrm{S}}{d\mathrm{PO}_2}\right)^2\right]$$
$$\nabla\mathrm{PO}_2.\left(\frac{[\mathrm{Hb}]}{\alpha}\nabla\frac{d\mathrm{S}}{d\mathrm{PO}_2}\right) \qquad (11)$$

Equations (9)–(11) represent the complete non-linear blood oxygen transport model, referred to herein as Model 1, which incorporates both the free oxygen and bound oxygen. Previous studies have used simpler models in order to reduce computational expense. Firstly, the non-linearity can be removed by replacing $d\mathrm{S}/d\mathrm{PO}_2$ with a constant mean value of $\overline{d\mathrm{S}/d\mathrm{PO}_2}$ calculated using Eq. (12)[19]:

$$\overline{\frac{d\mathrm{S}}{d\mathrm{PO}_2}} = \left(\frac{n\overline{\mathrm{S}}}{\overline{\mathrm{PO}_2}}\right)\left(1 - \overline{\mathrm{S}}\right) \qquad (12)$$

where $\overline{\mathrm{PO}_2}$ is a mean reference value fixed at 75 mmHg and replaces PO_2 in the Hill equation in order to evaluate $\overline{\mathrm{S}}$, as shown in Eq. (13):

$$\overline{\mathrm{S}} = \frac{\overline{\mathrm{PO}_2}^n}{\overline{\mathrm{PO}_2}^n + \mathrm{PO}_{2,50}^n} \qquad (13)$$

Secondly, the dispersion of the RBCs can be ignored by setting $D_c = 0$, and finally, the bound oxygen can be completely disregarded by setting $[\mathrm{Hb}] = 0$.

Similar to the study by Moore and Ethier[19] the following five models were compared:

Model 1 Both the free and bound oxygen are modeled and the non-linearity of the Hill equation is retained.

Model 2 Both the free and bound oxygen are modeled and the non-linear element, $d\mathrm{S}/d\mathrm{PO}_2$, is replaced with the constant value $\overline{d\mathrm{S}/d\mathrm{PO}_2}$ evaluated using Eq. (12).

Model 3 Both the free and bound oxygen are modeled and the non-linearity of the Hill equation is retained, but $D_c = 0$, thus neglecting the shear-augmented dispersion of RBCs.

Model 4 Both the free and bound oxygen are modeled and the non-linear element, $d\mathrm{S}/d\mathrm{PO}_2$, is replaced with the constant value $\overline{d\mathrm{S}/d\mathrm{PO}_2}$, and $D_c = 0$.

Model 5 Only the free oxygen is modeled, i.e. $[\mathrm{Hb}] = 0$.

Arterial Wall Oxygen Transport

The arterial wall consists of three layers: the intima, media and adventitia. In this study only the two inner layers, i.e. the intima and media, are included in the arterial wall models with distinct transport parameters assigned to each based on a study by Richardson.[23] In this study, the convection by the interstitial fluid in the arterial wall is ignored as the convective velocity of interstitial fluid is two orders of magnitude lower than the diffusive velocity.[19] It is also assumed that the endothelial cells lining the artery offer no resistance to the oxygen transport,[27] and as oxygen diffuses through the arterial wall it is consumed by the cells within.[29] The consumption rate of oxygen within the wall can be affected by a number of different variables, e.g. thickness of arterial wall, presence of inflammation/atherosclerotic plaque, subject species and age.[23] For the purposes of this study the Michaelis–Menten Kinetics model was employed to model the oxygen consumption within the arterial wall:

$$M = M_0 \frac{\mathrm{PO}_2}{\mathrm{PO}_2 + \mathrm{PO}_{2,M}} \qquad (14)$$

where M is the consumption rate of oxygen, M_0 is the maximum consumption rate and $\mathrm{PO}_{2,M}$ is the value of PO_2 at which the rate of reaction is half-maximal.[22] The resultant diffusion equation employed for the prediction of the transport of oxygen in the arterial wall is:

$$\frac{d\mathrm{PO}_2}{dt} = \nabla.(D_T\nabla\mathrm{PO}_2) - \frac{M}{\alpha_T} \qquad (15)$$

where D_T is the diffusivity of oxygen and α_T is the solubility of oxygen in the arterial wall tissue. Unless otherwise stated the values listed in Table 1 were used for the parameters in all simulations and the boundary conditions are given at the end of each test case description.

TABLE 1. List of parameter values used for the blood and arterial wall oxygen transport model.

Symbol	Units	Blood	Intima	Media	Reference
α	$ml_{O_2}/ml_{blood}/mmHg$	3.0×10^{-5}	–	–	Pittman[21]
D_b	m^2/s	1.2×10^{-9}	–	–	Moore and Ethier[19]
[Hb]	ml O_2/ml blood	0.2	–	–	Pittman[21]
$PO_{2,50}$	mmHg	26	–	–	Ethier[19]
n	–	2.7	–	–	Hill[12]
D_T	m^2/s	–	0.9×10^{-9}	1.05×10^{-9}	Richardson[23]
α_T	$ml_{O_2}/ml_{tissue}/mmHg$	–	2.4×10^{-5}	2.4×10^{-5}	Richardson[23]
M_0	$ml_{O_2}/ml_{tissue}/s$	–	2.1×10^{-5}	1.21×10^{-5}	Richardson[23]
$PO_{2,M}$	mmHg	–	1	1	Goldman[9]

Test Cases

To compare the five different blood oxygen transport models two separate test cases were devised. Test Case 1 compares the transarterial wall PO_2 profiles predicted in an idealized carotid bifurcation using the fives models with measurements recorded by Santilli *et al.* in dog carotid bifurcations.[25] In Test Case 2 the maximum and minimum transarterial wall PO_2 profiles in a stented coronary artery predicted using the five models were compared with measurements from a separate study by Santilli *et al.* In this separate study transarterial wall PO_2 profile measurements were taken within rabbit aortae, of similar size to human coronary arteries, which had been implanted with 3 mm stents.[26] Additionally, the PO_2 and the local Sherwood number, Sh, on the stented artery luminal surface predicted by each model were compared, along with the percentage volume of the arterial wall exposed to low and hypoxic levels of PO_2. Finally, in Test Case 3 the most advanced model, Model 1, was applied to the three sample stents to demonstrate how different stent designs can impact the oxygen transport within a stented coronary artery.

Test Case 1: Carotid Bifurcation

Santilli *et al.* used an oxygen microelectrode to measure the transarterial wall PO_2 gradients in 11 dog carotid bifurcations.[25] Although these measurements from Santilli *et al.* are from dog arteries, they are used for comparison with the predicted results for a human with the distance through the arterial wall scaled according to the thickness of the human artery. The five different models were used to simulate the oxygen transport in an idealized carotid bifurcation, shown in Fig. 2, adapted from Tada with the addition of a heterogeneous arterial wall.[16,17,28] The geometry, constructed in Rhinoceros 3D (McNeel, Indianapolis, IN, USA), comprised of the common carotid artery (CCA) which bifurcates into the internal carotid artery (ICA) and the external carotid artery (ECA). To reduce computational expense the geometry was halved along
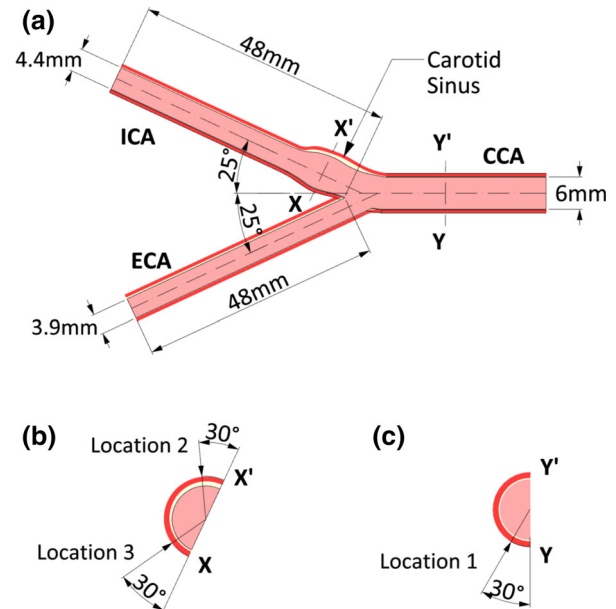
FIGURE 2. (a) Plan of the carotid bifurcation model with (b) cross-section *X–X'* and (c) cross-section *Y–Y'*. The intima thickness is approximately 0.12 mm throughout the common carotid artery (CCA) and the internal carotid artery (ICA), except in the outer wall of the carotid sinus and proximal to the ICA where it gradually increases to a maximum of 0.63 mm in accordance with Ku *et al.*[16] This can be seen clearly in the cross-section *X–X'*.

the centreline of the carotid arteries, thus ignoring the secondary curvature of the ICA.[28] The thickness of the arterial wall in the carotid arteries, particularly the intima in the carotid sinus, has been shown to vary with location in human subjects.[16] Accordingly, a variable intimal thickness ranging from 0.10 to 0.63 mm was used, as shown in Fig. 2, which corresponds to the mean values of measurements from biplanar angiographs from 57 patients as listed by Ku *et al.*[16] The media was assumed not to experience any thickening and was assigned a constant thickness of 0.60 mm. The predicted and measured transarterial wall PO_2 profiles were then compared at three of the six measurement locations as outlined by Santilli
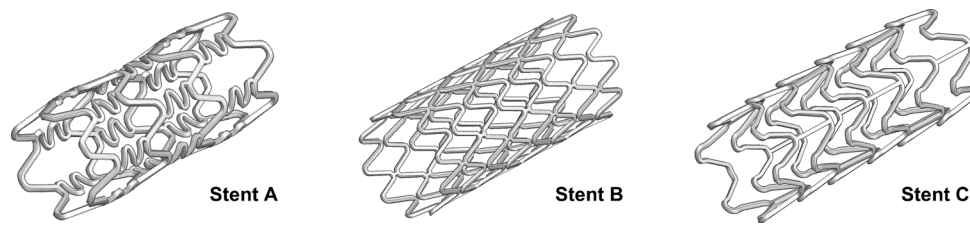
FIGURE 3. The three stents analyzed. The final deformed configuration is shown.

TABLE 2. Geometrical properties of the three investigated stents.[18]

Stent	A	B	C
Stent configuration	Closed-cell	Open-cell	Open-cell
Strut thickness	0.14 mm	0.10 mm	0.13 mm
Strut width	0.13 mm	0.10 mm	0.10 mm
Link configuration	Peak-to-peak	Peak-to-peak	Peak-to-valley
Link type	Flexible	Non-flexible	Non-flexible
Link shape	N-shaped	Straight	Straight
Link width	0.10 mm	0.08 mm	0.10 mm

et al.[25] One of the benefits of these locations numbered 1–3, in terms of assessing the blood oxygen transport models, is that they cover three distinct flow patterns: straight shear flow parallel to a wall, low shear recirculation flow and high shear flow directed towards the wall, respectively.

Boundary Conditions
A mass flow rate boundary condition of 0.00375 kg/s was placed at the inlet of the CCA which corresponds to the averaged mass flow rate over the cardiac cycle, divided by two for the half geometry, as taken from a study by Tada.[28] Additionally, at the inlet $PO_{2,in} = 100$ mmHg, which corresponds to the average luminal value recorded by Santilli et al.,[25] and also the typical arterial value found in human arteries.[22] At both outlets $PO_{2,out} = 0$ mmHg and an entrainment boundary condition was imposed with a zero relative pressure. The mass flow rates at the two outlets were compared with the calculated transient mass flow rates from Tada and found a maximum difference of 5.68% in the averaged flow rate over the cardiac cycle at ECA outlet. At the external wall boundary, which corresponds to the medial/adventitia interface, a constant $PO_2 = 75$ mmHg was imposed, which was the averaged PO_2 value recorded at the adventitia by Santilli et al. At the arterial wall surfaces located at the inlet and outlets a zero flux PO_2 boundary condition was imposed.

*Test Case 2 and Test Case 3: Stented Coronary Artery*

Three different stent designs, shown in Fig. 3, were investigated in this study and are referred to as Stent A, Stent B and Stent C with their differing geometrical properties listed in Table 2.[18] Stent A resembles the BX Velocity stent (Cordis of Johnson & Johnson, Fremont, CA, USA). Stent B resembles the S7 AVE stent (Medtronic, Fridley, MN, USA) and Stent C resembles the thick strut Multilink RX Ultra stent (Abbott Laboratories, North Chicago, IL, USA). Only Stent A was used for comparison of the five different blood oxygen transport models in Test Case 2. All three stents were compared using the most advanced model, i.e. Model 1, in Test Case 3 for the purpose of demonstrating the effects of different stent geometries on the PO_2 values within the arterial wall. The realistically-deformed stented artery geometries were obtained from non-linear finite element analyzes (FEA) carried out using ABAQUS (Dassault Systèmes, Providence, RI, USA). These structural analyzes consisted of the expansion of the sample stents using a realistic model of a tri-folded balloon-tipped catheter within an idealized coronary artery as shown in Fig. 4. The thicknesses of the intima and media were 0.24 and 0.32 mm, respectively, as adopted from Holzapfel et al.[13] The details of these analyzes are discussed elsewhere.[18] Figure 5 shows the surface mesh within the stented region for all three stents to give an indication of the mesh density employed here in the CFD-oxygen transport analyzes.

Boundary Conditions
For the stented artery models the following boundary conditions were implemented. At the inlet of the fluid domain a fully developed Hagen-Poiseuille velocity profile was imposed with $V_{mean} = 0.2313$ m/s and $PO_{2,in} = 100$ mmHg, which is normal arterial blood
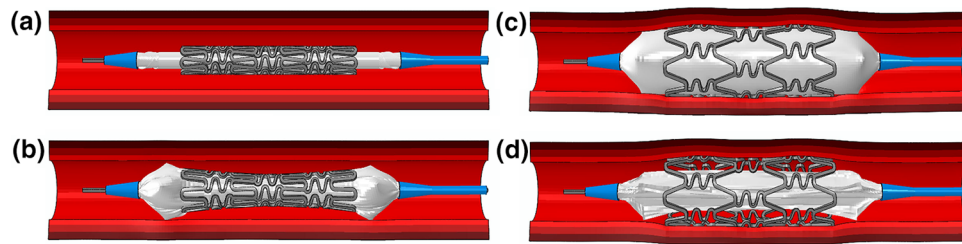
FIGURE 4. FEA-predicted deployment of Stent A using a tri-folded balloon-tipped catheter within an idealized coronary artery with a heterogeneous multi-layered arterial wall incorporating an intima, media and adventitia.[18] (a) Initial configuration with a pressure load = 0.00 MPa (b) expansion of balloon with a pressure load = 0.50 MPa, (c) maximum expansion with a pressure load = 1.10 MPa, and (d) the final deformed configuration with a pressure load = −0.01 MPa.

PO_2.[22] At the outlet an entrainment boundary condition with a zero relative pressure was set with $PO_{2,out} = 0$ mmHg. PO_2 was free to transfer across the luminal/arterial wall surface and on the stent surface a PO_2 zero-flux condition was imposed. On the media/adventitia interface surface $PO_2 = 45$ mmHg, as used by Richardson,[23] and on the wall surfaces located at the inlet and outlet a zero flux boundary condition was imposed.

Discretisation of Computational Domains

A structured mesh topology was used to discretise the computational domain for Test Case 1, while an unstructured mesh topology was used for Test Case 2. These were generated using ANSYS ICEM meshing software (ANSYS Inc., Canonsburg, PA, USA). The mesh for Test Case 1 was comprised of hexahedral elements and the mesh for Test Cases 2 was comprised of tetrahedral and prism elements. Following mesh convergence studies for each test case, the resultant meshes had total node counts of 1566030 and 2639580 for Test Cases 1 and 2 respectively. The meshing parameters applied in Test Case 2 were used for each of the three sample stents analyzed in Test Case 3.

Modeling the Blood Flow

The meshes were imported into the CFD commercial software ANSYS CFX 15 (ANSYS Inc., Canonsburg, PA, USA) where the Navier–Stokes equations were solved to predict the blood flow within the luminal domain. All simulations were steady state as pulsatility has been shown to have a minimal effect on oxygen transport to the arterial wall.[15] The density of blood was taken as 1060 kg/m³ and the non-Newtonian nature of blood was modeled using the non-Newtonian Bird–Carreau model with assigned values based on experimental data from Jung *et al.*[14] The momentum and continuity equations were solved with a high resolution advection scheme and the convergence criteria were set to a maximum residual tolerance

of 1×10^{-6}. All simulations were carried out on the Irish Centre for High-End Computing (ICHEC) Fionn supercomputer using a maximum of five nodes, each with 2×12 2.4 GHz Intel Ivy Bridge core processors and 64 GB of RAM.

Modeling the Oxygen Transport

The PO_2 in the blood and the arterial wall is represented in ANSYS CFX 15 as an additional variable. Additional variables are defined in ANSYS CFX as non-reacting scalar components that are transported through a flow field but do not affect the momentum or continuity equations. The transport of the PO_2 within the blood flow is governed by Eq. (9) with flow variables affecting the transport through the $\mathcal{D}PO_2/\mathcal{D}t$ term. The diffusivity coefficient, D', is represented by Eq. (10) and the source term is controlled by Eq. (11). Both D' and the source term are evaluated explicitly, based on the previous time step value for PO_2, and a time step independence study found no difference in results at lower time step values. The PO_2 is transported *via* diffusion only in the arterial wall with a fixed diffusivity coefficient, D_T, and consumption modeled *via* a source term. The advection/diffusion equation for PO_2 in the lumen domain was solved with a high resolution advection scheme, in line with recommendations by Carroll *et al.*,[4] and the convergence criteria were set to a maximum residual tolerance of 1×10^{-6} in all domains.

Variable of Interest: Sherwood Number

Sh is a dimensionless mass-transfer coefficient and was calculated using the predicted results in Test Cases 2 and 3 along the luminal surface using:

$$Sh = -\frac{\text{Dia}\left(dPO_2/dn\right)}{(PO_{2,in} - PO_{2,w})} \quad (16)$$

where Dia is the diameter of the artery, dPO_2/dn is the gradient of PO_2 normal to the wall, $PO_{2,in}$ is the PO_2
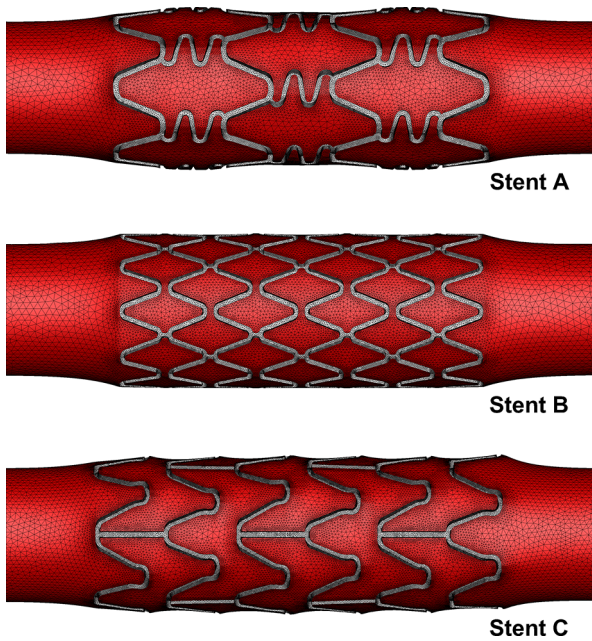
FIGURE 5. Surface mesh used for the stent and luminal surface for the three stents analyzed.

set at the inlet and $PO_{2,w}$ is the PO_2 predicted at the arterial wall luminal surface. Low Sh highlights potential areas on the luminal surface where the underlining cells may be in danger of hypoxia. To establish what constitutes low Sh the Damkholer number (dimensionless reaction rate coefficient) is first calculated using:
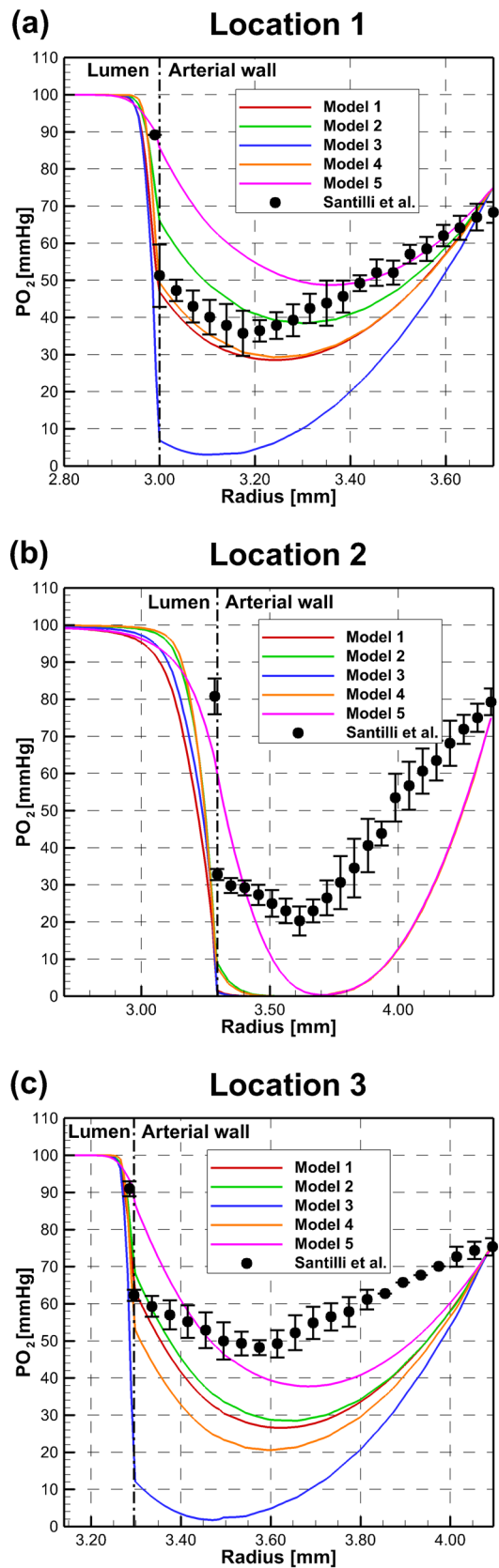
$$Da = \frac{M_0 T \text{Dia}}{\alpha_T D_T PO_{2,\text{in}}} \quad (17)$$

where T is the arterial wall thickness. Using the assigned parameters for the coronary artery models presented here the calculated $Da \approx 17$. When $Sh \gg Da$ the supply exceeds the demand within the arterial wall; however, as $Sh \rightarrow Da$ the PO_2 levels become increasingly dependent upon the blood oxygen transport.[29] Therefore, as the Sh drops towards this calculated value of Da the PO_2 levels within the arterial wall will decrease to possible hypoxic levels.

RESULTS AND DISCUSSION

Test Case 1

The results of each model at all three locations within the human carotid bifurcation are presented in Fig. 6 along with experimental values recorded by Santilli *et al.* in dog carotid bifurcations. Models 1–4, which include the bound oxygen, predict a steep gra-

dient within the mass-transfer boundary layer at Locations 1 and 2 that is also observed between the luminal and first arterial wall PO₂ value in the experimental results from Santilli *et al.* Model 5, which does not include the bound oxygen fails to predict this steep gradient. The reasoning for this steep gradient is presented below.

Previous studies have explained this steep gradient in PO₂ between the lumen and arterial wall as due to high oxygen consumption by the endothelium,[31] and this is currently an unresolved controversy in this field because it is not corroborated by *in vitro* studies. This controversy is covered in depth by both Vadapalli *et al.* and Tsai *et al.*[30,32] In the results presented here, predictions by Model 1 show that the steep gradient seen experimentally could be due to the complex balance between the free and bound oxygen contained within the mass-transfer boundary layer, and the consumption within the arterial wall. This could be a very

important consideration for future oxygen transport studies.

As an example, the PO₂, dS/dPO₂, D' and S values for each model are shown in Fig. 7 for the boundary layer at Location 1. Model 1 and 3 include the non-constant gradient of the dissociation curve, dS/dPO₂, in the calculation of D'. As shown in Fig. 7b, dS/dPO₂, increases rapidly within the boundary layer which numerically results in a decreased D' within this region for both Model 1 and 3. What this means physiologically is that there are two exchanges taking place: the exchange of oxygen between the blood and the arterial wall, and the exchange of oxygen between the RBCs and the plasma; i.e., the bound and free oxygen. The free oxygen only constitutes 1.5% of the total oxygen contained within the blood[22] and therefore, the bound oxygen can have a significant effect on the exchange of oxygen between the blood and the wall. This is exemplified by the difference in PO₂ between the models that include the bound oxygen, Models 1–4, and the one that does not, Model 5. Additionally, for Model 3 where the dispersion of the RBCs, which generally increases the oxygen flux, is ignored ($D_c = 0$) and the non-linear relationship between the free and bound oxygen there is a significant drop in the predicted PO₂ levels at the luminal surface.
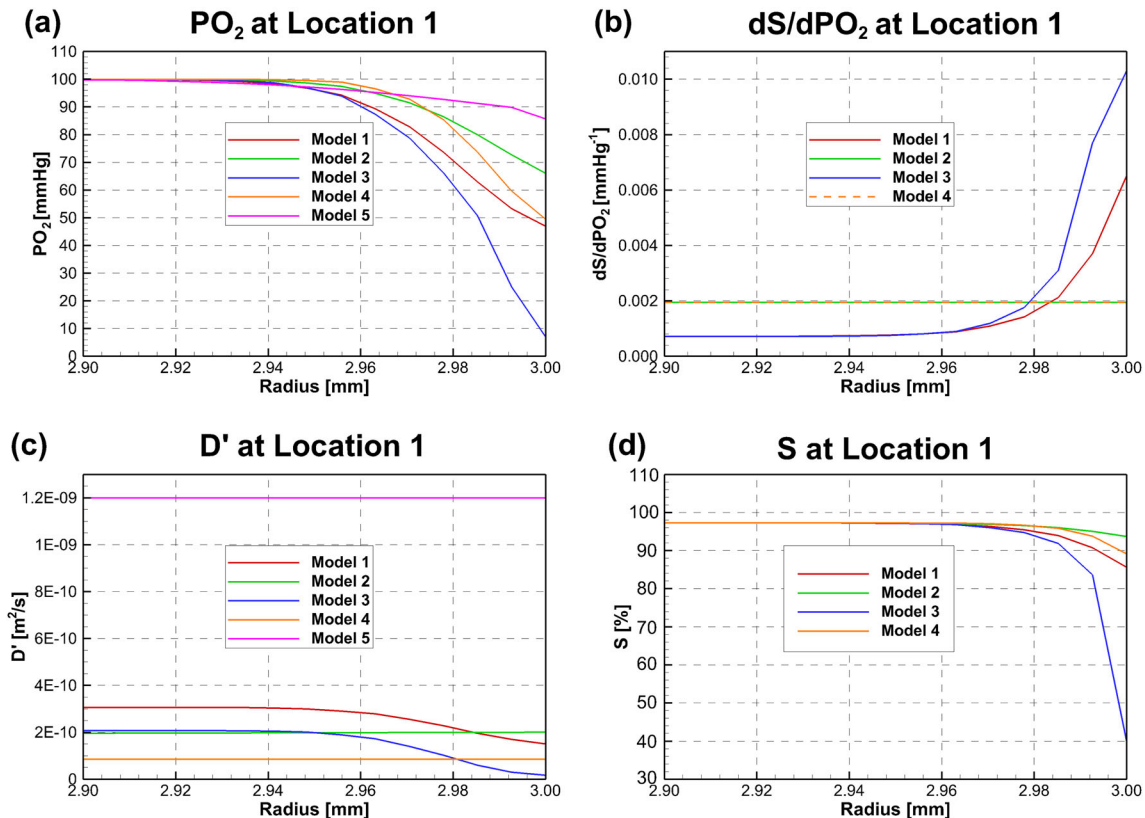
FIGURE 7. Predicted (a) PO₂, (b) dS/dPO₂,(c) D' and (d) S values along a line within the blood flow from a radius of 2.9 mm to the luminal surface at a radius of 3.0 mm at Location 1 for Test Case 1.

(a) Maximum Transarterial PO$_2$ Profile
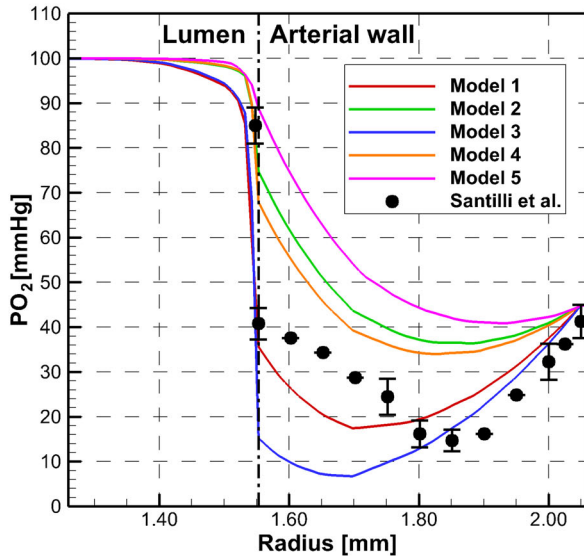
(b) Minimum Transarterial PO$_2$ Profile
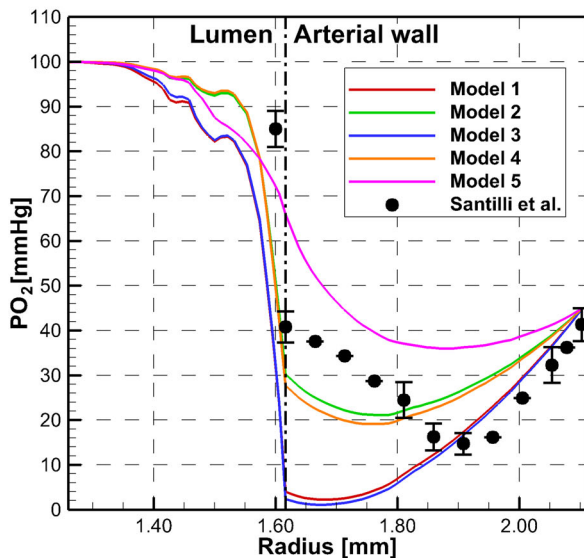
FIGURE 8. (a) Maximum and (b) minimum transarterial PO$_2$ profiles for each model applied to the deformed coronary artery geometry virtually implanted with Stent A. Measurements adapted from Santilli et al. are shown for comparison and the distances through the arterial wall for these have been scaled to the size of a human coronary artery.[26] The minimum PO$_2$ luminal surface value for each model is located within a recirculation zone immediately downstream of a stent strut which produces a severe drop and variable slope in PO$_2$ profile in (b). The luminal surface is shown as a vertical dashed-dotted line.

In terms of the PO$_2$ transarterial profiles in the arterial wall for Model 1 at Location 1 the predicted PO$_2$ values show reasonable agreement with the experimental results in capturing the overall trend. At

Location 2 there is a considerable difference. There are several reasons for this, all stemming from the fact that in humans this location is commonly a site of intimal thickening, caused by atherosclerotic plaque build-up, as included here. Conversely, in dogs, as studied by Santilli et al., the wall thicknesses are actually thinner at this location compared with Location 1 (154.0 ± 4 μm at Location 2 vs. 203.7 ± 5.5 μm at Location 1).[25] The intimal thickening in humans takes place over an extended period of time and would result in the penetration of vasa vasorum into the medial layer which increases the oxygen supply to the cells at this site.[33] What is seen in the PO$_2$ predictions presented here for Location 2 is the consequence of the thickening without penetration of the vasa vasorum. Additionally, as described by Richardson, the fat content and stage of atherosclerotic plaque build-up within the intima affects both the consumption rate and the solubility of oxygen within the arterial wall.[23] Therefore, to properly predict the PO$_2$ profile at this location more information is needed on the effects of plaque build-up on the oxygen diffusion and consumption. Lastly, at Location 3 the predicted PO$_2$ value just within the arterial wall matches well with the experimental results from Santilli et al.; however, the PO$_2$ values across the arterial wall differ with those recorded experimentally, which again would be due to differences in consumption, diffusion and solubility of the oxygen at this location.

The predicted results using the other four models show a broad variation in comparison with Model 1. At Locations 1 and 2 Model 2 gives a higher luminal surface value than Model 1. Linearising the dS/dPO$_2$ term generally produces a higher D' value within the mass-transfer boundary layer whose effect is to allow more oxygen to diffuse through to the luminal surface and is most pronounced at Location 1 for Model 2. At Location 3, where the flow is directed towards the arterial wall, the PO$_2$ value within the boundary layer is close to the value taken for $\overline{PO_2}$, which explains why there is relatively little difference between Models 1 and 2 at this location. Model 3 which has the lowest D' values, consistently under-predicts the PO$_2$ values across the arterial wall at all locations. Model 5 with a relatively high D' value is shown to over-predict the PO$_2$ at all locations.

Test Case 2

Figures 8a and 8b show the maximum and minimum PO$_2$ transarterial profile plots within the stented domain for all five models which were taken at the position of maximum and minimum luminal surface values. For comparison the measurements by Santilli

et al. from rabbit aortic arteries on day 1 following stent implantation with 3 mm internal-diameter stents are also shown.[26] The stents used were manufactured by Cordis, although it was not stated specifically that the BX Velocity stent was used. The balloon used was a 3 mm outer diameter balloon, which was also used in the FEA simulations presented here. In their study, the exact measurement location within the stented domain is not provided and therefore, the maximum and minimum profiles for each model are presented here alongside the experimental results. Assuming the experimental results are taken as being reflective of the values present in a similar size human coronary artery, as modeled here, then Model 1 is again shown to produce the steep PO_2 gradient and is within the range of luminal surface PO_2 values observed experimentally. Differences in the PO_2 transarterial profile could be attributed to differences in arterial wall properties of different species.

Contour plots of the PO_2 and Sh are shown in Figs. 9a and 9b respectively. When analyzed in conjunction with the line plots along the axial cross-section A–A' (Fig. 10) the effects of each model become apparent. The difference between Model 1 and the simpler models is striking. Firstly, the plots of the PO_2 values along the luminal surface in Fig. 9a show quite a large variability across the five models with the extent of the difference clear in the PO_2 line-plot in Fig. 10. The areas of low PO_2 values (<30 mmHg) around the stent struts which are apparent with Model 1 do not

appear with Models 2, 4 and 5, with Model 5 predicting very little variation in PO_2 on the luminal surface with the lowest value being 64 mmHg. Model 3, which neglects the RBC dispersion predicts exceedingly low PO_2 levels on the luminal surface which translates into very little PO_2 diffusing into the arterial wall. Interestingly though, Model 3 predicts very high Sh values along the surface because the Sh is based on the gradient of PO_2 normal to the surface, which is very high for Model 3 as seen in Fig. 8 previously. This highlights a possible disadvantage in using the Sh as a basis for analysis.

The relatively small variation in PO_2 values observed along the luminal surface for Model 5 translates to very little variation predicted in the local Sh also. For Models 1–4 there is a similarity in the regions of low and high Sh, with low Sh (values tending towards the calculated $Da \approx 17$) predicted in regions where the flow is separating away from the luminal surface and high Sh predicted in regions where the flow is reattaching, i.e. where the flow is directed towards the wall and oxygen transport through convection is high. The peaks of high Sh observed with Models 1–4 are dampened considerably for Model 5 to the extent that the reattachment points are unrecognizable on the luminal surface plots.

Greater amounts of neointimal thickening have been shown to occur in areas with PO_2 values of less than 30 mmHg and hypoxia exists where the PO_2 levels drop to below 10 mmHg.[6,26] Thus, how much of the
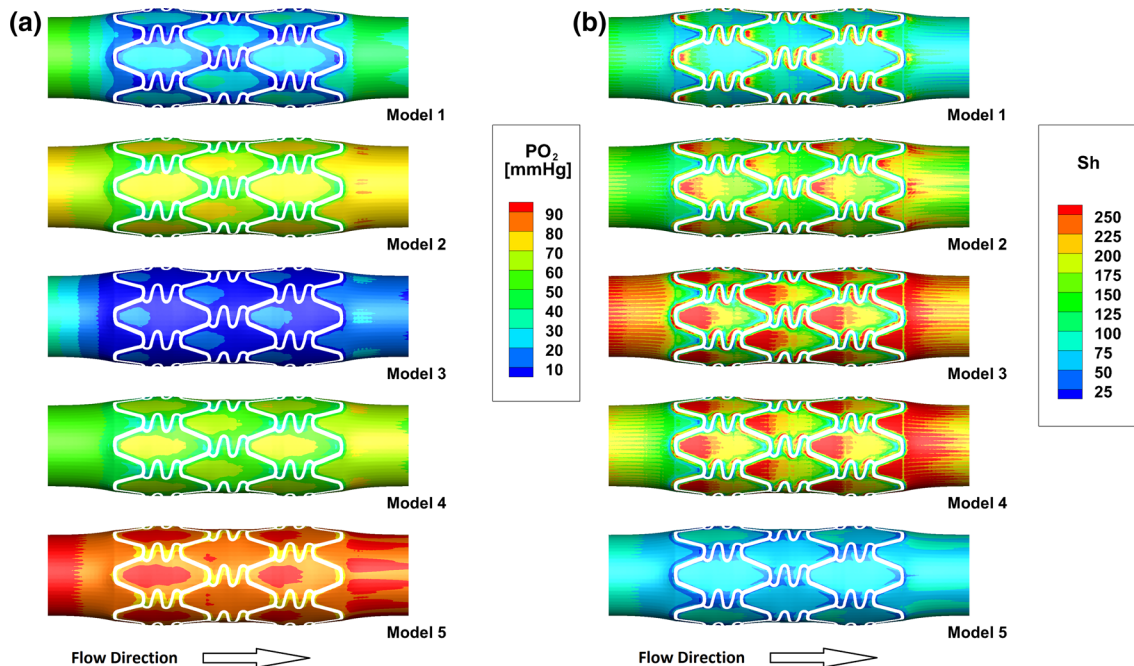

FIGURE 9. Predicted (a) PO_2 and (b) Sh using all five models on the stented artery luminal surface for Stent A.
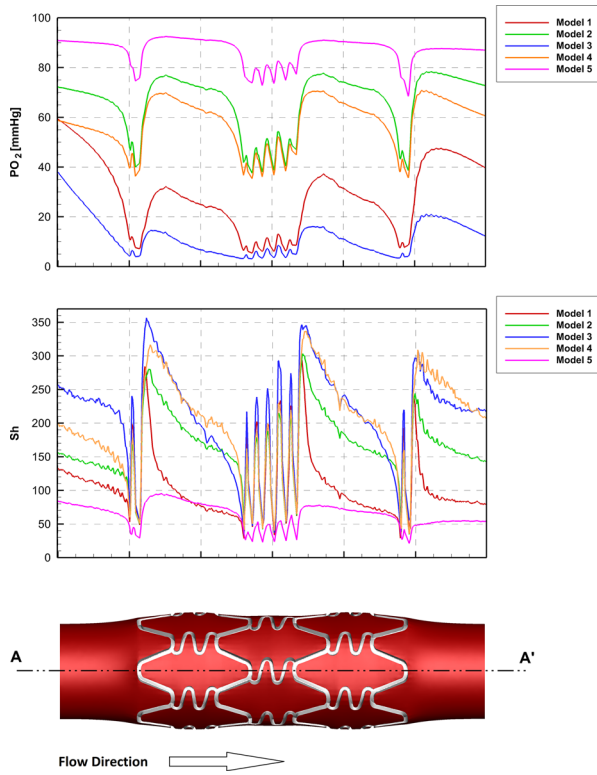
FIGURE 10. Predicted PO_2 and Sh using all five models along line A–A' for Stent A

TABLE 3. Percentage volume of the arterial wall exposed to hypoxic and low PO_2 within the stented region for each model along with the minimum and maximum D' values present within the blood flow.

	Hypoxic PO_2 (<10 mmHg) (%)	Low PO_2 (<30 mmHg) (%)	D'_{min} (m²/s)	D'_{max} (m²/s)
Model 1	16.28	76.9	1.12E−11	3.51E−10
Model 2	0.0	15.0	9.05E−11	2.56E−10
Model 3	45.6	85.3	6.13E−12	2.08E−10
Model 4	0.0	35.0	8.58E−11	8.58E−11
Model 5	0.0	0.0	1.20E−09	1.20E−09

arterial wall is exposed to PO_2 values below these two thresholds is of importance in predicting the possibility of excessive neointimal thickening and potential ISR. As shown in Table 3, the five models studied here predict a broad range of percentage volumes of the arterial wall exposed to low PO_2 (<30 mmHg). For example, Model 5 predicts that none of the stented arterial wall is exposed to low PO_2, as opposed to Model 1 predicting 76.9% of the stented arterial wall is exposed to low PO_2 with 16.3% exposed to hypoxic conditions. Critically, this again highlights the disadvantages of simplifying the blood oxygen transport model.

Test Case 3

The PO_2 and Sh luminal surface plots and PO_2 axial cross-sectional plots for Stents A, B and C are presented in Figs. 11 and 12. Immediately apparent in Figs. 11a and 12 is that the N-shaped link struts in Stent A, which are predominantly aligned perpendicular to the flow, cause an extended region of recirculation zones and consequently low PO_2 values on the luminal surface. This in turn results in the extremely high percentage volume of the arterial wall at 76.9% exposed to low PO_2 and 16.3% of the arterial wall being exposed to hypoxic conditions, as listed in Table 4. Stent B has the second highest percentage volume exposed to low PO_2 at 69.5%. Crucially though, only 4.6% of the arterial wall is exposed to hypoxic conditions for Stent B. Stent C performs the best of the three stents with only 60.1% of the arterial wall exposed to low PO_2 and only 1.9% exposed to hypoxic conditions. When Fig. 12 is analyzed it becomes apparent that the design of Stent C, with stent struts that are well-spaced out and link struts which are aligned with the flow, results in reduction in the size of the low and hypoxic PO_2 zones. As shown in Table 4, it is not simply a case of decreased lumen/arterial wall interface area within the stented region which impinges the PO_2 flux into the arterial wall. This further suggests the dominance of the augmented haemodynamic environment caused by stent implantation on the oxygen flux. Interestingly, the prolapse of the arterial wall between the struts allows increased oxygen convection into the wall downstream of each strut, which is apparent in Fig. 9b with high Sh in these regions. This detail would not have been captured effectively with an idealized non-deformed arterial wall.

The angiographic restenosis rates for each commercially available coronary stent that resemble the three stents are presented in Table 4, along with the percentage volume of the arterial wall exposed to low and hypoxic PO_2 levels. These rates were taken from the following clinical trials at 6-month follow-up: Stent A, ISAR-STEREO-II, Stent B, DISTANCE and Stent C, ISAR-STEREO-I. Stent A is predicted to perform the worst in terms of volumetric percentages of low and hypoxic PO_2 within the arterial wall and interestingly, it also shows the highest restenosis rate. Stents B and C are predicted to both have significantly less percentage volume of the arterial wall exposed to hypoxic PO_2 levels and both show lower restenosis rates in comparison with Stent A. Stent C is predicted to perform the best out of the three stents; however, this does not match with the restenosis rates. Considering ISR is a multifactorial process, there may be some other issue with this stent, e.g. structural damage of the
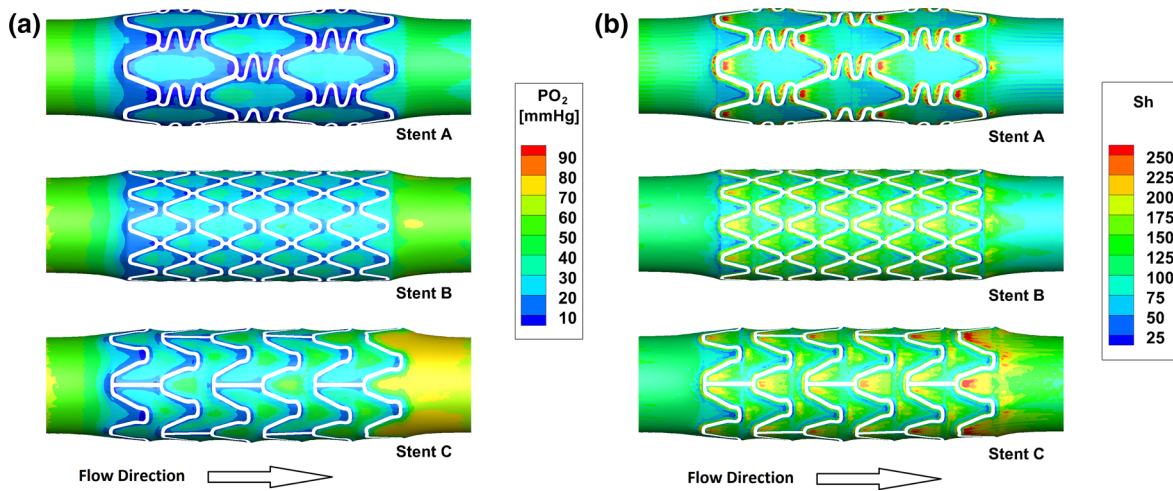
FIGURE 11. Predicted (a) PO$_2$ and (b) Sh on the stented artery luminal surface for the three stents analyzed.

TABLE 4. Percentage volume of the arterial wall exposed to low and hypoxic PO$_2$ within the stented region for each stent along with restenosis rate and lumen/arterial wall interface area within the stented region.

Stent	A	B	C
Low PO$_2$ (<30 mmHg) (%)	76.9	69.5	60.1
Hypoxic PO$_2$ (<10 mmHg) (%)	16.3	4.6	1.9
Restenosis rate (%)	31.4	10.1	25.8
Interface area (mm^2)	99.75	95.43	99.11

arterial wall or areas of low wall shear stress, which is not captured by oxygen transport models alone.

LIMITATIONS

In terms of limitations of the methodology and possible avenues for future work, the shear-dependant dispersion of RBCs is a haemodynamic flow feature that is not fully understood. This may be improved by particle based CFD software which could model all the constituent cells of blood including the RBCs. Additionally, at low shear rates RBCs are known to form rouleaux which could impact both their dispersion and the oxygen transport. Therefore, future studies of this phenomenon may improve the predictive capability of the model. All the simulations carried out as part of this study were steady state and the assumption of rigid arterial walls was used. Including pulsatile flow and wall motion may be an avenue for future studies. Also, the haematocrit is considered to be constant throughout the fluid domain when in reality there would be a reduced haematocrit within the plasma skimming layer at the luminal surface. This could affect the predicted steep gradient in the PO$_2$ levels within the blood adjacent to the luminal surface, although to what extent would need further investiga-
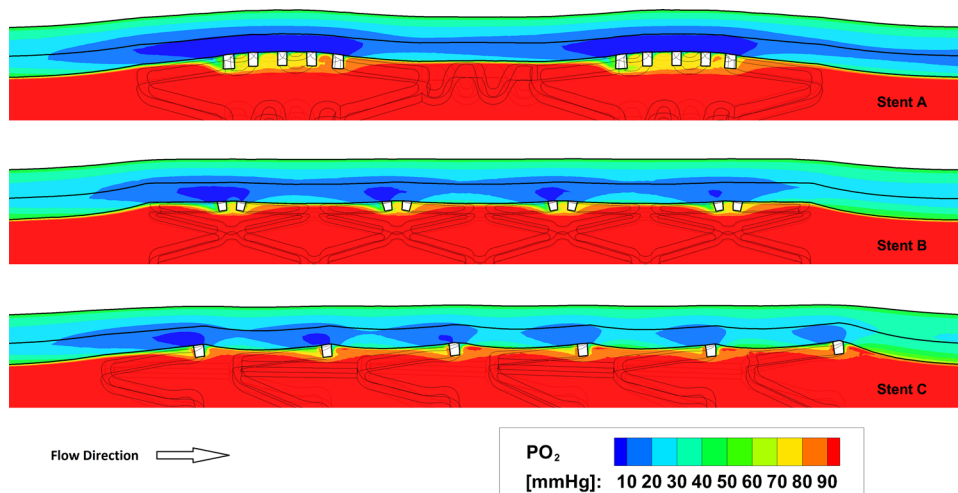

FIGURE 12. Axial cross-section of predicted PO$_2$ in both the arterial wall and lumen within the stented region for the three stents analyzed. The interfaces between all three domains are clearly outlined.

tion. Additionally, one aspect which was not varied was the parameters defining the oxygen transport within the arterial wall. In reality, for stented arteries the presence of plaque, and additionally the structural damage caused to the arterial wall by stent implantation, could result in a much higher oxygen demand within the arterial wall. Thus, the values shown here in this study are conservative estimates of the PO_2 levels and in reality the situation could be significantly worse. Clearly, as shown by the results at Location 2 in Test Case 1, more accurate representations of each layer of the arterial wall, including plaque, and their diffusion/reaction parameters based on cellular composition would be required for more patient-specific analysis; unfortunately, these are not available at present. Given the aforementioned correlations between hypoxia and IH, with the addition of patient-specific geometries and parameters this methodology could be a considerable aid to the both the design of future implantable devices and also to the tailored analysis of the impact of these devices on individual patients.

CONCLUSIONS

Three important conclusions for future analyzes of oxygen transport in stented arteries are inferred by this study. Firstly, ignoring the oxyhemoglobin content within the RBCs leads to large errors in the PO_2 gradient within the mass-transfer boundary layer and, consequently, the prediction of hypoxic regions within the arterial wall. The standard simplified model which ignores oxyhemoglobin, i.e. Model 5, and is crucially the most commonly used model in the literature, over-predicts the PO_2 levels in both the carotid bifurcation and stented coronary artery test cases presented here. It therefore presents an overly optimistic view of the risk of IH caused by low and hypoxic PO_2 levels. Secondly, neglecting the shear-induced dispersion of RBCs also affects the accuracy of the predicted results. Thirdly, given the link between IH and hypoxia as concluded by other studies, numerical modeling of oxygen transport in arteries using Model 1 could offer a powerful tool in predicting the safety of any future implanted devices or procedures which impact the haemodynamic, and consequently the oxygen transport, environment within the arterial system.

ACKNOWLEDGEMENTS

REFERENCES

[1]Camenzind, E., P. G. Steg, and W. Wijns. Stent thrombosis late after implantation of first-generation drug-eluting stents: a cause for concern. *Circulation* 115:1440–1455, 2007; (discussion 1455).

[2]Caputo M, C. Chiastra, C. Cianciolo, *et al.* Simulation of oxygen transfer in stented arteries and correlation with in-stent restenosis. *Int J Numer Method Biomed Eng.* 29:1373–1387, 2013.

[3]Caro, C. G., T. J. Pedley, R. C. Schroter, and W. A. Seed. Mechanics of the Circulation. Oxford: Oxford University Press, 1978.

[4]Carroll, G. T., P. D. Devereux, D. N. Ku, T. M. McGloughlin, and M. T. Walsh. Experimental validation of convection-diffusion discretisation scheme employed for computational modelling of biological mass transport. *Biomed Eng Online.* 9:34, 2010.

[5]Cha, W., and R. L. Beissinger. Evaluation of shear-induced particle diffusivity in red cell ghosts suspensions. *Korean J. Chem. Eng.* 18:479–485, 2001.

[6]Cheema, A. N., T. Hong, N. Nili, *et al.* Adventitial microvessel formation after coronary stenting and the effects of SU11218, a tyrosine kinase inhibitor. *J. Am. Coll. Cardiol.* 47:1067–1075, 2006.

[7]Coppola, G., and C. G. Caro. Arterial geometry, flow pattern, wall shear and mass transport: potential physiological significance. *J. R. Soc. Interface* 6:519–528, 2009.

[8]Diller, T. E. Comparison of red cell augmented diffusion and platelet transport. *J. Biomech. Eng.* 110:161–163, 1988.

[9]Goldman, D. Theoretical models of microvascular oxygen transport to tissue. *Microcirculation.* 15:795–811, 2008.

[10]Goldsmith, H. Red cell motions and wall interactions in tube flow. *Fed Proc.* 30:1578–1590, 1971.

[11]Goldsmith, H., and J. Marlow. Flow behavior of erythrocytes. II. Particle motions in concentrated suspensions of ghost cells. *J. Colloid Interface Sci.* 71:383–407, 1979.

[12]Hill A V. The possible effects of the aggregation of the molecules of haemoglobin on its dissociation curve. *J Physiol.* 41:iv–vii, 1910.

[13]Holzapfel, G. A., R. W. Ogden, C. Lally, and P. J. Prendergast. Simulation of In-stent Restenosis for the Design of Cardiovascular Stents. Berlin Heidelberg: Springer, pp. 255–267, 2006.

[14]Jung, H., J. W. Choi, and C. G. Park. Asymmetric flows of non-Newtonian fluids in symmetric stenosed artery. *Korea Aust Rheol J.* 16:101–108, 2004.

[15]Kolandavel, M. K., E.-T. Fruend, S. Ringgaard, and P. G. Walker. The effects of time varying curvature on species transport in coronary arteries. *Ann. Biomed. Eng.* 34:1820–1832, 2006.

[16]Ku, D. N., D. P. Giddens, C. K. Zarins, and S. Glagov. Pulsatile flow and atherosclerosis in the human carotid bifurcation. Positive correlation between plaque location and low oscillating shear stress. *Arteriosclerosis.* 5:293–302, 1985.

[17]Ma, P., X. Li, and D. N. Ku. Convective mass transfer at the carotid bifurcation. *J. Biomech*. 30:565–571, 1997.

[18]Martin, D. M., E. A. Murphy, and F. J. Boyle. Computational fluid dynamics analysis of balloon-expandable coronary stents: influence of stent and vessel deformation. *Med. Eng. Phys*. 36:1047–1056, 2014.

[19]Moore, J. A., and C. R. Ethier. Oxygen mass transfer calculations in large arteries. *J. Biomech. Eng*. 119:469–475, 1997.

[20]Murphy, E. A., and F. J. Boyle. Reducing in-stent restenosis through novel stent flow field augmentation. *Cardiovasc Eng Technol*. 3:353–373, 2012.

[21]Pittman, R. N. Regulation of tissue oxygenation. *Colloq. Ser. Integr. Syst. Physiol. Mol. Funct*. 3:1–100, 2011.

[22]Popel, A. S. Theory of oxygen transport to tissue. *Crit. Rev. Biomed. Eng*. 17:257–321, 1989.

[23]Richardson, R. B. Age-dependent changes in oxygen tension, radiation dose and sensitivity within normal and diseased coronary arteries-Part B: modeling oxygen diffusion into vessel walls. *Int. J. Radiat. Biol*. 84:849–857, 2008.

[24]Sanada, J.-I., O. Matsui, J. Yoshikawa, and T. Matsuoka. An experimental study of endovascular stenting with special reference to the effects on the aortic vasa vasorum. *Cardiovasc. Intervent. Radiol*. 21:45–49, 1998.

[25]Santilli, S. M., R. B. Stevens, J. G. Anderson, W. D. Payne, and M. D. Caldwell. Transarterial wall oxygen gradients at the dog carotid bifurcation. *Am. J. Physiol. Hear Circ. Physiol*. 268:H155–H161, 1995.

[26]Santilli, S. M., A. S. Tretinyak, and E. S. Lee. Transarterial wall oxygen gradients at the deployment site of an intraarterial stent in the rabbit. *Am. J. Physiol. Heart Circ. Physiol*. 279:H1518–H1525, 2000.

[27]Stangeby, D. K., and C. R. Ethier. Computational analysis of coupled blood-wall arterial LDL transport. *J. Biomech. Eng*. 124:1–8, 2002.

[28]Tada, S. Numerical study of oxygen transport in a carotid bifurcation. *Phys. Med. Biol*. 55:3993–4010, 2010.

[29]Tarbell, J. M. Mass transport in arteries and the localization of atherosclerosis. *Annu. Rev. Biomed. Eng*. 5:79–118, 2003.

[30]Tsai, A. G., P. Cabrales, and M. Intaglietta. The physics of oxygen delivery: facts and controversies. *Antioxid. Redox Signal*. 12:683–691, 2010.

[31]Tsai, A. G., P. C. Johnson, and M. Intaglietta. Oxygen gradients in the microcirculation. *Physiol. Rev*. 83:933–963, 2003.

[32]Vadapalli, A., R. N. Pittman, and A. S. Popel. Estimating oxygen transport resistance of the microvascular wall. *Am. J. Physiol. Heart Circ. Physiol*. 279:H657–H671, 2000.

[33]Vavuranakis, M., F. Sigala, D. A. Vrachatis, *et al*. Quantitative analysis of carotid plaque vasa vasorum by CEUS and correlation with histology after endarterectomy. *Vasa*. 42:184–195, 2013.